Journal of Power Sources 492 (2021) 229636

Contents lists available at ScienceDirect

Journal of Power Sources

journal homepage: www.elsevier.com/locate/jpowsour

The effects of cycling on ionic and electronic conductivities of Li –ion battery electrodes

Fezzeh Pouraghajan [a], Andrea I. Thompson [a], Emilee E. Hunter [a], Brian Mazzeo [b], Jake Christensen [c], Ram Subbaraman [c], Michael Wray [d], Dean Wheeler [a,*]

[a] Department of Chemical Engineering, Brigham Young University, Provo, UT, 84602, USA
[b] Department of Electrical & Computer Engineering, Brigham Young University, Provo, UT, 84602, USA
[c] Robert Bosch LLC, Research and Technology Center, Palo Alto, CA, 94304, USA
[d] K2 Energy Solutions, Inc., Henderson, NV, 89011, USA

HIGHLIGHTS

- Ionic and electronic resistances were directly measured.
- Electrodes were tested in pristine, formed, and cycled conditions.
- Electronic resistivity always increases with cycling.
- Ionic resistivity is stable and may even decrease unless temperature is elevated.

ARTICLE INFO

Keywords:
Cycle aging
Ionic conductivity
Electronic conductivity
Tortuosity

ABSTRACT

Li-ion battery performance is dependent on ionic and electronic transport, in turn dependent on electrode microstructure. Changes in microstructure during cell formation and cycling are poorly understood. In this work, the changes in effective ionic conductivity and diffusivity are quantified in terms of MacMullin number, a dimensionless ionic resistance that is related to tortuosity. Using an AC impedance technique, namely the blocking electrolyte method, the ionic resistance of electrode films at varying extents of cycling was determined. Variations in electronic resistivity were quantified by micro-scale measurements using a previously developed micro-four-line probe. Cycling effects on the ionic and electronic resistivity were investigated for a graphite anode and multiple cathode chemistries including $LiCoO_2$ (LCO), $LiNi_xCo_yMn_zO_2$ (NCM), and $LiFePO_4$ (LFP). Clear evidence of changes in ionic and electronic resistivity were observed during cell formation and cycling. The magnitude of the changes depended on the chemistry of the electrodes and cycling conditions. The results indicate that, under normal cycling conditions, electronic resistivity increases while ionic resistivity is relatively stable and in some cases decreases, the latter being unexpected. However, under accelerated (high-temperature) cycling conditions, both electronic resistivity and ionic resistance were observed to increase.

1. Introduction

Li-ion batteries are well-established as energy storage devices due to their high energy densities, low self-discharge, and long cycle life. Current battery life is satisfactory for many applications, whereas for others, such as electric vehicles, stationary energy storage, or satellites, higher cycle life and a longer lifespan are desired [1]. In order to achieve a longer lifespan for Li-ion batteries, it is necessary to better understand the most significant of the many complex processes that lead to cell aging or deterioration.

Cell aging occurs during both passive storage and active cycling. Aging during storage, also called calendar aging [2,3], is due to thermodynamic instability of the materials. Cycling additionally leads to degradation due to changes in active material state of charge and the presence of electrochemical gradients [4]. One generally observes over a cell's lifetime two main changes: capacity fade and impedance growth [5–9]. In this work, we seek to understand how much this impedance growth during cycling is attributable to changes in ionic and electronic

* Corresponding author.
E-mail address: dean_wheeler@byu.edu (D. Wheeler).

https://doi.org/10.1016/j.jpowsour.2021.229636
Received 22 September 2020; Received in revised form 3 February 2021; Accepted 8 February 2021
Available online 24 February 2021
0378-7753/© 2021 Elsevier B.V. All rights reserved.

transport properties of the electrodes, which in turn depend on the microstructure.

Tortuosity and porosity of the electrode are two commonly used indicators of microstructure. In this work, the ratio of intrinsic electrolyte conductivity (k_{in}) to effective conductivity (k_{eff}) is used to determine the MacMullin number (N_M), which with known porosity (ε) can be used to determine tortuosity (τ). The MacMullin number can also be defined as the ratio of intrinsic electrolyte diffusivity (D_{in}) to effective diffusivity (D_{eff}). These relationships can be summarized as

$$N_M = \frac{\tau}{\varepsilon} = \frac{k_{in}}{k_{eff}} = \frac{D_{in}}{D_{eff}} \quad (1)$$

To our knowledge, there have been no previous direct measurements of electrode ionic and electronic transport properties during cell aging. Such information can assist efforts to mitigate electrode deterioration and inform physics-based lifetime models.

In order to provide an overview of different battery degradation mechanisms and to link these processes to microstructural changes in electrodes, some of the main aging phenomena are here briefly introduced. Battery aging can originate from either chemical or mechanical degradation mechanisms [10]. Chemical degradation mechanisms are mainly associated with unwanted side reactions that result in electrolyte decomposition, passive film formation, gas formation, and active material dissolution [11,12]. Mechanical degradation mechanisms, on the other hand, are associated with mechanical stress and strain due to the volume changes during Li (de)-intercalation processes [13].

In a negative electrode (anode), the main contributor to the impedance growth is considered to be the solid electrolyte interphase (SEI) [14,15]. The SEI is intrinsically a resistive layer whose growth will therefore raise the local impedance of the electrode [5]. Another aging mechanism in the anode active material is attributed to the volume changes due to Li-ion insertion and extraction. These volume changes can impose mechanical stress and strain to the active material and cause particle fracture and loss of contact between different components of the electrode [16,17].

Mechanisms that are known to contribute to cathode aging include structural changes during cycling and chemical decomposition and dissolution reactions [10,18]. These mechanisms are complicated and interdependent. Their sensitivity to cell chemistry and cell design means they may vary from manufacturer to manufacturer [13]. The volume change and phase transitions accompanying Li-ion (de)intercalation can lead to microcracks, loss of electrical contact between particles and between particles and the current collector, which consequently leads to an increase in impedance of the cell [13,16,19–23]. It has been shown that such structural changes can have a more significant effect on the cathode performance compared to a carbonaceous anode [24], even though the volume change of cathode active materials is typically lower than that of graphite.

Active material dissolution is another aging mechanism in positive electrodes, particularly with Mn-based active material. In addition to the loss of positive electrode capacity, dissolved transition metals tend to migrate to the anode side and incorporate into the SEI, increasing the electronic conductivity of the layer. Electron leakage in turn accelerates SEI growth which contributes to further increases in cell impedance and capacity fade [25]. However, the exact mechanism of this effect on the SEI layer is still under debate [26,27]. A mechanism proposed by Delacourt et al. suggests Mn^0 is present in the SEI, allowing for higher conductivity. Trapped Mn also reversibly reacts with Li and causes a severe structural and morphological change of the SEI layer during cycling leading to further electrolyte decomposition and SEI growth [26]. Another mechanism proposed by Zhan suggests Mn^{2+} ions in the electrolyte react with the mobile Li^+ ion in the SEI and subsequently block the lithium diffusion path which leads to an increase in graphite impedance and capacity fade [25].

Another factor that can influence electrode microstructure is binder and carbon black migration. A study on Li(Ni,Mn,Co)O_2/graphite cells cycled at high temperature by Bodenes et al. showed poly (vinylidenefluoride) (PVDF) binder migration from the outer layer of the positive electrode toward the negative electrode [28]. Their study revealed significant changes within the microstructure of the electrode, which was due to the nonhomogeneous distribution of the binder as a result of binder migration. Likewise, Striebel et al. observed the presence of disordered carbonaceous material on the surface of aged anode attributed to carbon black additive migration from the composite cathode to the anode [29].

The focus of this work is to study changes in electrode tortuosity and electronic resistivity caused by battery aging during cycling. In order to obtain tortuosity values, we used the blocking-electrolyte method [30] introduced by Gasteiger and coworkers [31] in which a non-intercalating electrolyte is used to determine effective ionic transport through the electrode film. In order to obtain microscale electronic resistivity measurements, we used the previously fabricated micro-four-line probe and measurement inversion technique [32].

Li-ion battery performance depends on the choice of active materials and cell design and manufacturing process; aging mechanisms are influenced by these factors. In order to have a more broad understanding of cycling's effect on electrode transport properties, both an anode and cathodes with different chemistries from different format cells commonly used in the industry were chosen for this study. Cathode chemistries included lithium cobalt oxide (LCO), lithium nickel cobalt manganese oxide (NCM), lithium iron phosphate (LFP), and a blend of transition metal oxides (TMO). Electrodes were tested at different stages of battery health: (1) pristine electrodes which had never been in contact with battery electrolyte, (2) formed electrodes harvested from newly-assembled cells, and (3) cycled electrodes harvested from repeatedly cycled cells. Due to the disparate commercial sources, some testing protocols necessarily differed from one cell type to another. In the cases of LCO and blended TMO cathodes, electrodes were fully cycled, harvested, and then sent to us, whereas for the cases of LFP and NCM, cells were cycled in our laboratory.

2. Experimental overview

2.1. Symmetric pouch cell assembly

Because electrodes that were harvested from battery cells contain dried lithium salts and ethylene carbonate, a rinsing procedure was used to remove any residues. This rinsing procedure is iportant for the blocking-electrolyte method since it is necessary to avoid any intercalation of residual lithium salts.

Dimethyl carbonate solvent was specifically chosen for the rinsing process as it is a component of the battery electrolyte, to prevent any possible undesired interactions. The electrodes were soaked in a dimethyl carbonate solvent for at least 12 h. The electrodes were then removed and the conductivity of the waste solvent was measured. This process was repeated until the conductivity of the waste solvent was found to be vanishingly small. The electrodes were then dried.

In order to make blocking-electrolyte cells, electrodes and separators were placed into a pouch cell in a symmetric configuration. For larger samples, one 2 cm × 2 cm electrode and a second electrode (larger than 4 cm^2, to provide at least 1 mm overhang from all 4 sides) were cut. A separator (Celgard 3501, Celgard LLC, Charlotte, NC) was placed between these electrodes and the stack was placed into the pouch. Uncoated current collector tabs protruded from the pouch. For smaller samples, the electrode dimension was 1.5 cm × 1.5 cm. An electrolyte of 15 mM tetrabutylammonium hexafluorophosphate in a 1:1 (w:w) mixture of ethylene carbonate and diethyl carbonate was added to the pouch cell and the cell was sealed using a heat sealer. All of the salts and solvents used in these tests were obtained from Sigma Aldrich.

Ningde Amperex Tech. Exhibit No. 2030
Zhuhai CosMX Battery Co. Ltd. v. Ningde Amperex Tech.
IPR2025-00405, U.S. Patent No. 11,769,910
Page 2 of 9

2.2. Pouch cell testing

Blocking-electrolyte cells were tested by following the method explained in Pouraghajan et al. [12] for determining tortuosity. Using a Bio-Logic SP-200 potentiostat, electrochemical impedance spectra were measured around the open-circuit voltage of each cell. A frequency range of 0.5 Hz–1 MHz with a 10 mV perturbation was used for determining ionic resistances of the cells.

A differential-equation-based transmission-line model (TLM) was used to fit the effective ionic resistivity of the electrodes (R_{ion}), which was then used to determine the MacMullin number and tortuosity of the electrodes. Knowing R_{ion} based on the model, the MacMullin number (N_M) can be determined based on the cross-sectional area of the cell (A), the thickness of the sample (l), and the intrinsic conductivity of the electrolyte (k_{in}):

$$N_M = \frac{\tau}{\varepsilon} = \frac{R_{\mathrm{ion}} \cdot A \cdot k_{\mathrm{in}}}{l} \tag{2}$$

All pouch cells were tested under external compression of approximately 45 kPa. For each case, the measurements were repeated by making 4 pouch cells, in order to obtain a 95% confidence interval and average.

2.3. Electrode delamination

Delamination of the electrode films was achieved by soaking cathodes in 5–7 M potassium hydroxide solution. The electrodes were then rinsed with distilled water and allowed to dry.

2.4. Electronic measurement

A flexible micro-four-line probe was used to calculate the average electronic conductivities. This probe design is based on four-point-probe theory, where conductive lines are used instead of points [32,33]. The four-line probe takes tangential and orthogonal measurements, as shown in Fig. 1. For tangential measurements, a current is applied to the first line while the fourth line is connected to the ground. Then, the voltage is measured across the middle two lines. For orthogonal measurements, the same current is applied to the first and fourth lines while the current collector is connected to the ground. Then the voltage is measured between the middle lines and ground. From these measurements, bulk conductivity and contact resistance can be found using a mathematical model developed by Flygare et al. [34].

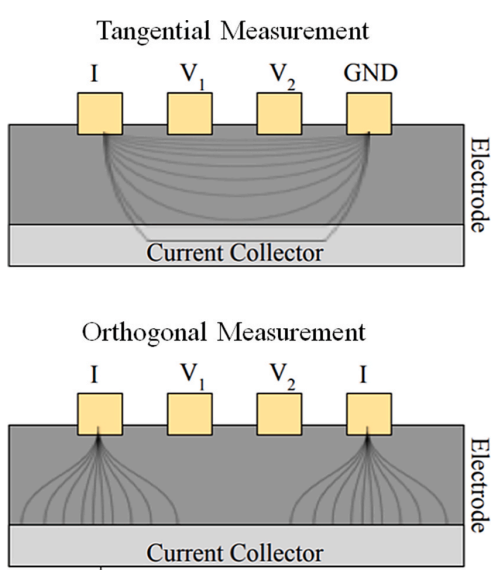

Fig. 1. Tangential and orthogonal measurement schematic.

2.5. Cell cycling and electrode harvesting

LCO cathodes were manufactured, cycled, and harvested by Hydro-Québec. Three different stages of electrodes were produced: pristine, formed, and cycled electrodes. The formed electrodes were harvested from a pouch cell that was cycled a few times. The cycled electrodes were harvested from a pouch cell cycled 180 times under accelerated life testing to 80% capacity at 1C rate, full-cell voltage range 3–4.4 V (vs. graphite), and at 55 °C. The cathode composition was 93 wt% LCO, 4 wt % carbon black (CB), and 3 wt% binder (dry basis).

For the remaining tested electrodes, the exact compositions are not reported, however as these electrodes are commercial electrodes we expect on the order of 2–4 wt% carbon black and a similar amount of binder (dry basis).

LFP cathodes were cycled and harvested at BYU from 18,650 cells provided by K2 Energy (1350 mAh). Cells were deep-cycled at 23–25 °C using a Maccor 4300, according to the following procedure: charge at 2C constant current to 3.8 V (vs. graphite) followed by a constant voltage step to 0.05C; discharge at 1C constant current to a cut-off voltage of 2.5 V followed by a constant voltage step to 0.05C. Cathodes were harvested from formed, 600-cycle and 1650-cycle cells.

Commercially available 2000 mA h cells (NCM/graphite) were cycled at BYU. Cells were deep-cycled 250, 600, and 850 times at 23–25 °C, and one cell was cycled 850 times at 50 °C. Cycling procedure included: charge at 2C constant current to 4.2 V followed by a constant voltage step to 0.05C; discharge at 2.5C constant current to a cut-off voltage of 2.5 V followed by a constant voltage step to 0.05C.

According to the manufacturer's product specification for (NCM/graphite) 18,650 cells, the temperature range for charging is 0–50 °C and for discharging is −20 to 80 °C and 90% capacity recovery after 3 months storage at −30 to 45 °C.

Cathodes containing a blend of NCA, NCM, and LMO were harvested from cycled prismatic automotive EV cells. A cell that was cycled at 3C rate inside an environmental chamber maintained at 25 °C (average cell temperature over cycling = 31 °C) retained 87% of original capacity after 1200 cycles. This cycling was aggressive relative to the cell's specification (max voltage < 4.15 V, cycling at C/2).

3. Results and discussion

3.1. Lithium cobalt oxide (LCO) cathode

Fig. 2-a, shows a slight expansion in the thickness of the LCO electrodes that causes porosity (Fig. 2-b) to increase for formed and cycled cathodes. Porosity values are calculated based on the mass loading of the cathode, its thickness, and the crystalline densities of the constituents [35].

We measured the MacMullin number of the LCO cathodes using the blocking-electrolyte method, as discussed in the experimental section. Fig. 2-c and 2-d compare MacMullin number and tortuosity values (with 95% confidence intervals) for pristine, formed, and cycled electrodes. There is a clear trend of increasing tortuosity with cycling. There are 4% and 49% increases in tortuosity of the formed and cycled cathodes, respectively. Based on the trend of increasing porosity, one would expect tortuosity to decrease over time, in accordance with the well-accepted Bruggeman relation [36]. There is some indication that this might be happening during the formation process. However, the observed increase in tortuosity and MacMullin number upon further cycling (Fig. 2-c and 2-d) is opposite to this expectation, meaning that the ionic pathways become more restrictive as the microstructure changes after formation and over time.

In addition, we measured electronic conductivity (Fig. 2-e) and contact resistance (Fig. 2-f) for pristine, formed, and cycled Hydro-

Ningde Amperex Tech. Exhibit No. 2030
Zhuhai CosMX Battery Co. Ltd. v. Ningde Amperex Tech.
IPR2025-00405, U.S. Patent No. 11,769,910
Page 3 of 9

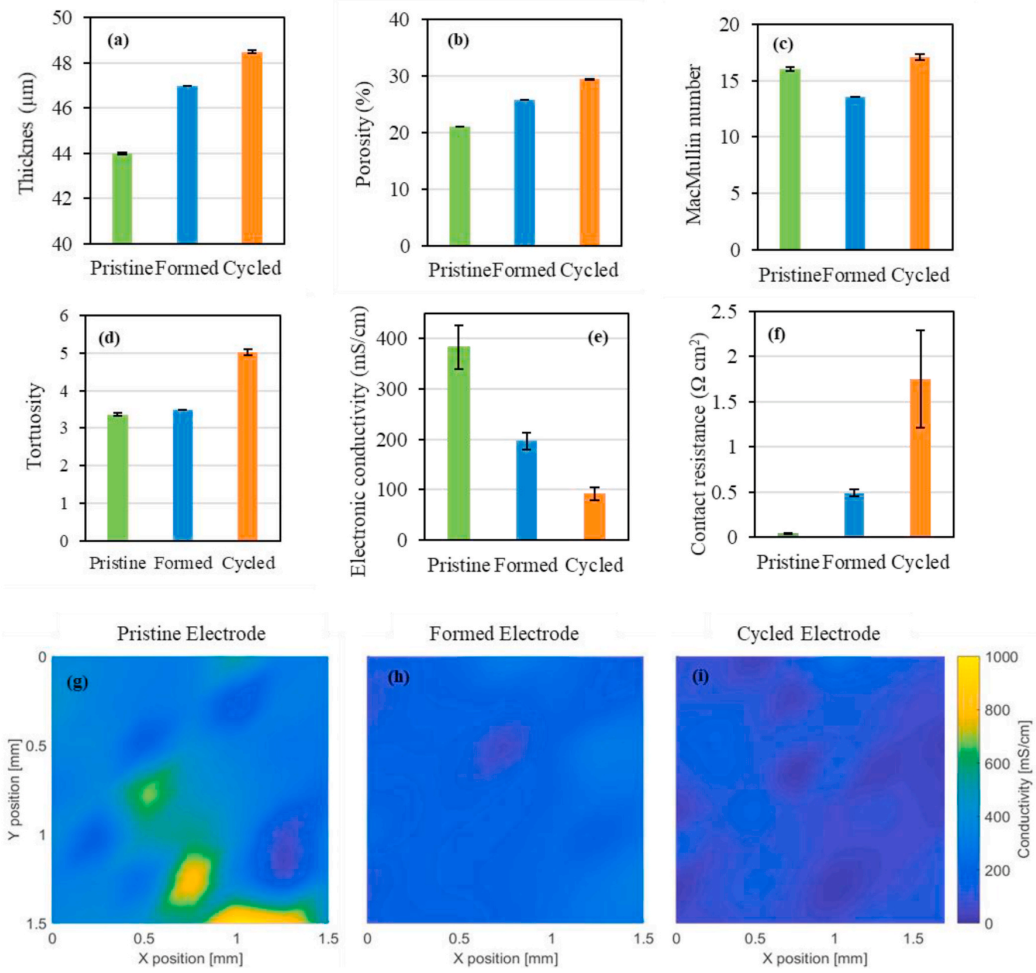

Fig. 2. Comparison for pristine, formed, and cycled LCO cathodes of (a) thickness, (b) porosity, (c) MacMullin number, (d) tortuosity, (e) electronic conductivity, and (f) contact resistance. Local electronic conductivity map for (g) pristine, (h) formed, and (i) cycled LCO cathodes. 95% confidence intervals are also shown on the bar plots.

Québec electrodes. The results show that electronic conductivity decreased, and contact resistance increased with cycling, to a much greater degree than changes to ionic transport.

Observed contact resistances are qualitatively consistent between ionic and electronic measurements. As discussed by Pouraghajan et al. the high-frequency semi-circle for the blocking-electrolyte technique is an indicator of contact resistance between the current collector and electrode film [30]. Fig. 3 shows an increase in the size of the semicircles in the high-frequency region of the Nyquist plots that shows contact resistance increased with cycling, similar to the trend observed through

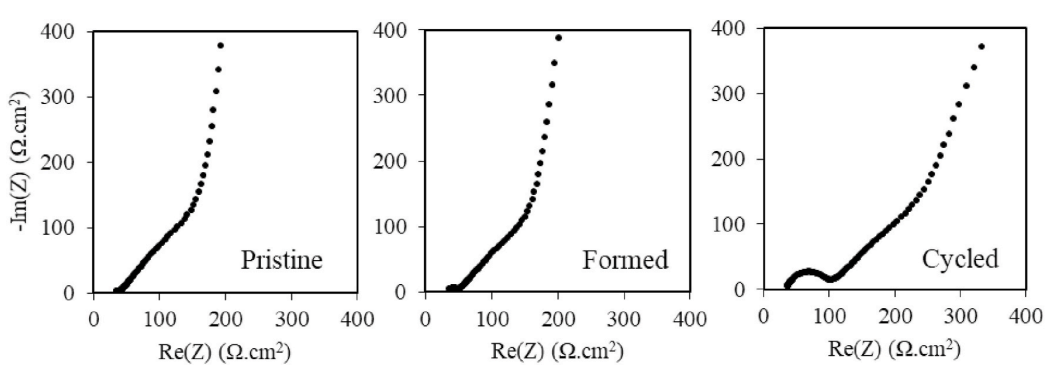

Fig. 3. Obtained Nyquist data of the blocking-electrolyte experiment for the pristine, formed, and cycled LCO cathodes, showing an increase in the size of the high-frequency semi-circle over time.

Ningde Amperex Tech. Exhibit No. 2030
Zhuhai CosMX Battery Co. Ltd. v. Ningde Amperex Tech.
IPR2025-00405, U.S. Patent No. 11,769,910
Page 4 of 9

electronic measurement in Fig. 2-f. Table 1 lists the values for "dry" contact resistance (Fig. 2-f)R_{con}, and high-frequency "wet" resistance obtained from the Nyquist plot, R_{hf}, for pristine, formed, and cycled electrodes. We previously observed that wet electronic resistivity of composite electrodes is greater than dry, by a factor of 2–3 for pristine electrodes [37]; however, the difference observed here between R_{hf} and R_{con} is greater than this upon cycling. Therefore, the high-frequency resistance appears to include resistances besides the contact resistance between the electrode film and the current collector, effects associated with introduction of electrolyte into the system.

A possible explanation for an increase in electronic resistances as cycling proceeds is that the electrode structure undergoes mechanical strain due to changes in molar volume as ions are inserted and removed [23]. This mechanical strain can result in loss of attachment and contact between active and carbon particles and binder. Mechanical strain can similarly cause partial delamination between the electrode film and the current collector, which leads to an increase in contact resistance [38].

Fig. 4 compares macroscale photographs of delaminated pristine, formed, and cycled electrodes. The delamination process was the same for each sample, as described in the experimental section. When the electrode film remains on the current collector, the current collector provides a large amount of mechanical support and the formed and cycled films look essentially the same as a pristine electrode. However, when the film is removed from the current collector, underlying mechanical changes become evident, as shown in Fig. 4. Localized degradation and damage such as ripples and rings on the cycled and formed electrodes are evidences of significant mm-scale heterogeneities. Cracks in the films observed in Fig. 4 likely happened during the delamination process, yet nevertheless indicate mechanical weakness not present in the pristine film.

The observed increase in tortuosity during cycling can be due to several effects, keeping in mind that the cell was cycled at 55 °C and charged to a higher voltage (4.4 V) than the typical charge voltage for LCO cells (4.2 V). Higher positive voltage and temperature increase the rate of the solvent oxidation reaction and accelerate CEI film formation [13,39–41]. There could also be active material dissolution and cracking. PVDF binder shows lower stability at higher potential and temperature, which causes more severe binder degradation [42–44]. This degradation may be associated with the observed heterogeneity in Fig. 4. Lastly, we must consider that carbon particle or binder migration could lead to non-uniform distribution of particles that could make the ionic path more tortuous. Although binder migration is known as a more significant issue during the drying step of electrode manufacturing [45, 46], it may happen to a lower extent during battery operation at higher temperatures [28]. Bodenes et al. showed PVDF binder migration from the positive to negative electrodes for cells cycled at high temperature and revealed significant microstructure changes due to the nonhomogeneous distribution of the binder [28]. Striebel et al. also observed evidence of carbon black additive migration from the composite cathode to the anode [29].

Any or all of the above mechanisms could block or partially obstruct pores and increase tortuosity. However, because the formation cycles were not done under aggressive conditions, we instead see stability or decrease in the MacMullin number for that part of the test, a result that is consistent with other electrodes discussed below.

Another way to analyze the results for these experiments is to compare the area-specific impedances attributable to ionic and electronic pathways. On average during a cell charge or discharge, an ion or electron moves through half of the electrode of thickness l. The area-specific resistance for ions to move through half of the electrode is $R_{\mathrm{ion}} = 0.5\, l/k_{\mathrm{eff}}$. The corresponding resistance for electrons is $R_{\mathrm{elec}} = 0.5\, l/\sigma$ where σ is the electronic conductivity of the electrode. These can be compared directly to the contact resistance reported in Fig. 2-f, R_{con}.

Table 1 summarizes all these resistances for LCO cathodes. Ionic resistance values are estimated based on an electrolyte with an intrinsic conductivity (k_{in}) of 10 mS/cm. When the results of the cycled electrode are compared against those for formed or pristine, it is evident that the relative change in bulk electronic resistance and contact resistance are much higher than the relative change in ionic resistance. This result suggests that the deterioration in the electronic pathway is more significant compared to the ionic one. However, for all three cases (pristine, formed, and cycled), bulk ionic resistance is still much larger than the measured dry electronic resistances and of bigger concern during high rate charge/discharge when ion depletion occurs due to diffusion effects [47].

Finally, we note that there is not a clear explanation of the largest resistance in Table 1 for cycled electrodes, namely R_{hf}. As previously mentioned, this resistance can be thought of as a "wet" version of the surface resistance R_{con}.The contact resistance is likely sensitive to the same factors that control bulk electronic resistance, namely the amount of conductive additive and microstructure. One effort to decouple these types of tradeoff is to use so-called gradient electrodes in which porosity and carbon additive are varied with position relative to the current collector have the biggest advantage in minimizing the contact resistance without unnecessarily increasing the others [48].

Table 1
Electronic, ionic, and contact resistances for LCO cathodes.

Resistance (Ω.cm^2)	Pristine	Formed	Cycled
R_{elec}	0.006 ± 0.001	0.012 ± 0.001	0.026 ± 0.003
R_{ion}	3.52 ± 0.04	3.19 ± 0.02	4.14 ± 0.07
R_{con}	0.045 ± 0.004	0.49 ± 0.04	1.75 ± 0.54
R_{hf}	~0	15.0 ± 1.4	61.3 ± 0.8

3.2. Lithium iron phosphate (LFP) cathode

Fig. 5-a shows a capacity decrease with cycling for the LFP cells. Fig. 5-b and 5-c, respectively, show ionic and electronic measurement results for LFP cathodes harvested from these cells. In contrast to LCO cathodes, no significant degradation of electronic and ionic conductivity was observed for these cathodes. Also, there was no significant change in the electrode thickness due to cycling. Figure S1 shows photographs of the delaminated cathodes from formed, 600-cycle, and 1650-cycle cells. There were not any observable signs of mechanical damage on the delaminated electrodes; however, the free-standing films tend to curl which could be an indication of the stress imbalances due to the strong cohesion of the coating. Qualitatively, the tendency of the free-standing film to curl decreased from the formed to 1650- cycle cathodes, which could be due to slight mechanical relaxation with cycling. Nevertheless, the results suggest that these electrodes maintained good structural stability following manufacturing. Note, however, there is a modest increase in the contact resistance of these electrodes as shown in Fig. 5-d. The observed increase in electronic conductivity (Fig. 5-c) does not have a good physical explanation and could be due to sample-to-sample variation, meaning the magnitude of the error bars are underestimated. Further, the change in conductivity for LFP is relatively small when compared to LCO, meaning the conductivity is relatively stable in this instance.

3.3. Lithium nickel cobalt manganese oxide (NCM) cathode

Fig. 6-a shows a capacity decrease with cycling for NCM cells. The cell cycled 850 times at 50 °C showed an additional 20% capacity loss compared to the cell cycled 850 times at room temperature. As expected, cycling at a higher temperature led to a more significant capacity loss.

Fig. 6-b (solid fill) shows a slight increase in the thickness of the cathodes as the number of cycles increases. The maximum expansion is 5% for the case of 850-cycle cathode at 50 °C. This expansion is expected as a result of degradation and strain during repetitive cycling.

Fig. 6-c (solid fill) shows the MacMullin number of the NCM

Ningde Amperex Tech. Exhibit No. 2030
Zhuhai CosMX Battery Co. Ltd. v. Ningde Amperex Tech.
IPR2025-00405, U.S. Patent No. 11,769,910
Page 5 of 9

Fig. 4. Photographs of the delaminated pristine, formed, and cycled LCO cathodes (approximate size 2.5 cm × 2.5 cm) showing mechanical damage increase as the cell cycles.

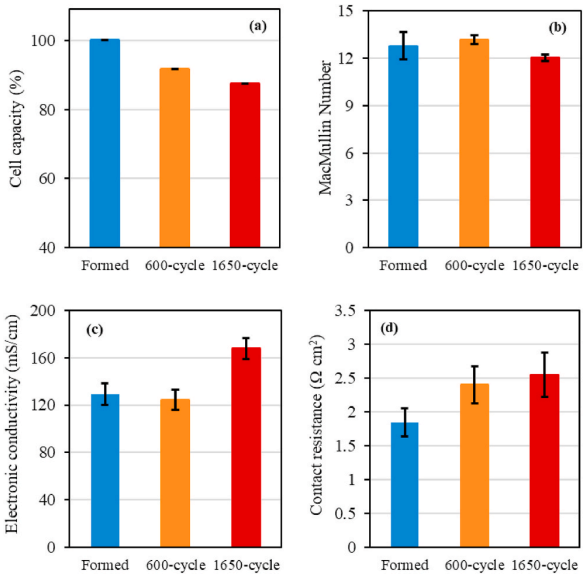

Fig. 5. LFP cathode properties as a function of aging, along with 95% confidence intervals for (a) cell capacity, (b) MacMullin number, (c) electronic conductivity, and (d) contact resistance.

cathodes. For cells that are cycled at room temperature, we observed decreasing MacMullin number with cycling. One might explain this as being caused by the modest increase in cathode thicknesses and hence porosity with cycling. However, comparing 850-cycle to formed cathodes, thickness increased 3.7% while MacMullin number decreased 27%. This observation suggests that the improved ionic pathway is not solely due to the increased porosity. Considering a correlation between tortuosity and porosity ($\tau = 1.8\varepsilon^{-0.53}$) proposed in Thorat et al. [49] work as an approximation, it can be concluded that half of the decrease in MacMullin number is caused by expansion of pore volume, and the other half is due to other mechanisms that opened up new ionic pathways. These mechanisms could include particle fracture, fragmentation of secondary particles, relaxation of polymer attachment between particles and other interfacial effects, and displacement of carbon and active particles [22–25].

Cycling at an elevated temperature is commonly used as an accelerated life testing procedure to predict or extrapolate cell behavior under long term cycling at normal temperature. Our results show that for the case of 850 cycles, MacMullin number of the cycled cathode at room temperature decreased 27% compared to the formed cathode, whereas cycling at the elevated temperature led to only a 14% decrease. If we assume that elevated temperature testing is an extrapolation of long term cycling, we would expect MacMullin number of 850-cycle at 50 °C to follow the decreasing trend and decline more than 27% rather than only 14%. This unexpected result suggests that different mechanisms are not accelerated to the same degree when aging a cell at elevated temperature. This temperature-related difference is also consistent with the observed decrease in ionic transport with accelerated (high-temperature) cycling of the LCO cathode above.

Fig. 6-d shows the electronic conductivity results at various cycling stages at room or elevated temperature. The results demonstrate that electronic conductivity decreased as the cycling proceeded at room temperature. At elevated temperature, the electronic conductivity of the cathode was lower than that at room temperature. This observation indicates that, as we expected, temperature increased the rate of degradation and had an adverse impact on electronic conductivity. The decreasing trend in electronic conductivity is likely due to general loss of structural integrity. While this effect causes electronic pathway deterioration in the bulk electrode, there is an associated loss in adhesion of the film to the current collector, increasing the contact resistance (Fig. 6-e). On the other hand, such structural changes in this case facilitated ion movement via decreased MacMullin number of the electrode as cycling proceeded.

Surprisingly, MacMullin number has less variation at elevated temperature than that at room temperature. Probably, besides the aforementioned degradation mechanism that improved ion pathways, another mechanism with an adverse effect occurred specifically at the elevated temperature. One possible mechanism would be cathodic film formation or binder morphological change, similar to what was proposed to explain changes in the LCO cathode. Therefore, it can be concluded that cycling at higher temperatures may not be an accurate extrapolation of a cell cycled at room temperature, even when both lead to the same capacity loss.

3.4. Graphite anode

Water-soluble-binder graphite anodes were harvested from the same (NCM/graphite) 18,650 cells discussed in the previous section. Fig. 6-b (patterned fill) shows an increase in the anode thickness as the number of cycles increased, which is similar to the trend observed for NCM cathodes. The maximum expansion was observed for the anode cycled 850 times at the elevated temperature, and the expansion was 8%.

Fig. 6-c (patterned fill) shows MacMullin number for the formed and cycled anodes at room or elevated temperature. There is a continuous decreasing trend in MacMullin number as the capacity of the cell decreases. Although SEI layer growth may deteriorate the ionic pathways and reduce the conductivity, it does not seem to have a noticeable role in this matter, or at least is overcome by other mechanisms that improve ionic pathways and decrease MacMullin number.

Fig. 6-c also shows that the graphite anode and cathode follow

Ningde Amperex Tech. Exhibit No. 2030
Zhuhai CosMX Battery Co. Ltd. v. Ningde Amperex Tech.
IPR2025-00405, U.S. Patent No. 11,769,910
Page 6 of 9

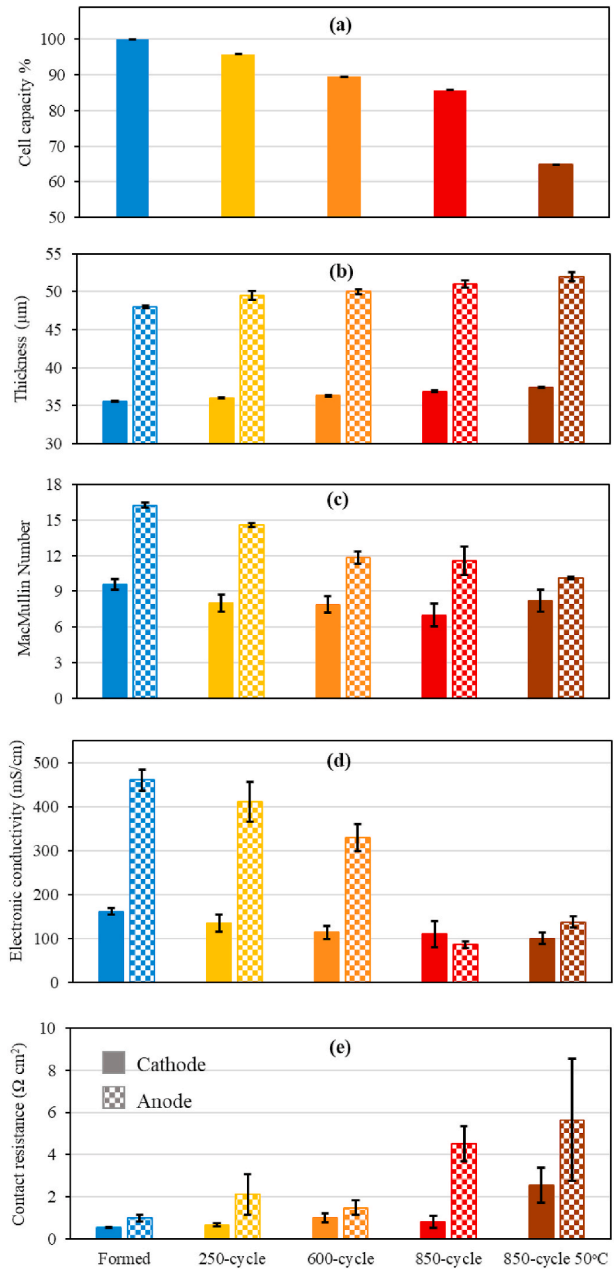

Fig. 6. NCM cathode (solid fill) and graphite anode (patterned fill) formed and cycled results with 95% confidence intervals for (a) cell capacity, (b) thickness, (c) MacMullin number, (d) electronic conductivity, and (e) contact resistance.

different trends for MacMullin number under the accelerated cycling condition. While the anode MacMullin number further decreased at the elevated temperature, MacMullin number of the cathode was higher at the elevated temperature, as described earlier. This observation clearly indicates that the temperature impact is different on the anode and cathode ionic conductivity.

Fig. 6-d (patterned fill) shows electronic conductivity variations for formed and cycled anodes. The results indicate that electronic conductivities of the anode reduced as the cycling proceeded. Interestingly, relative degradation in electronic conductivity is more significant in the graphite anodes compare to the NCM cathode.

Besides the differences in the binder materials and the nature of surface films (SEI vs. CEI), natural graphite also shows larger volume changes than cathode active materials during cycling [50]. This may lead to severe mechanical degradation in anode material, which in turn decreases the electronic conductivity of the anode more significantly. Kostecki's et al. observed gradual structural degradation of the graphite with cycling. Their Raman microscopy results indicate graphite structural disordering as a result of stresses associated with elevated temperature and numerous Li intercalation/deintercalation cycles [51,52].

The anode also had higher contact-resistance degradation compared to the cathode, as shown in Fig. 6-e. During disassembly of the cells, we observed partial delamination of the anode material, which became even worse over the course of cycling or with increasing the temperature. This adhesion problem would suggest an increase in contact resistance.

3.5. Blended TMO cathode from a commercial prismatic cell

The TMO (blend of NCM, NCA, and LMO) cathodes of the formed cell and 1200-cycle cell were compared. Furthermore, local tortuosity variations with cycling across the width of the cathodes of the commercial prismatic cells were tested (Fig. 7) to investigate possible local variation due to manufacturing or cycling.

Fig. 8-c shows the MacMullin numbers for the formed and cycled cathode at 7 regions along the width of the cathode. In addition to aging effects, the data show that the manufacturing process does not result in macroscopically uniform properties across the width of the electrode, similar to what was illustrated in Fig. 4. Fig. 8 shows the value of the MacMullin number was mostly consistent across the width of the formed cathode; however, starting at region 3, the MacMullin numbers of the cycled cathode deviated from those of the formed cathode. There is a clear correlation between electrode thickness (Fig. 8-b) and MacMullin number. Considering that loading density (Fig. 8-a) is consistent between the formed and cycled electrodes, we can conclude that the increase in the thickness is due to electrode swelling during cycling. The non-uniform change in MacMullin number suggests that one edge of the electrode underwent less significant aging compared to the rest. This non-uniform progression could be the result of non-uniform current density, temperature, and/or mechanical stress within the cell during cycling that lead to an uneven distribution of driving forces for aging.

Similar to the result obtained for NCM cathodes at room temperature, cycling of the blended electrode led to degradation and electrode expansion that facilitate ion transport through the electrode film. This phenomenon is accompanied by electronic pathway deterioration (Fig. 8-d) and contact resistance increase (Fig. 8-e) as expected.

Compared to what is observed in Fig. 4 little mechanical deterioration is observed for formed and cycled electrode after delamination. Figure S2 (Suplemental Material) shows delaminated cathodes from the formed and cycled cells.

4. Conclusions

Cycle aging was performed on different electrode chemistries

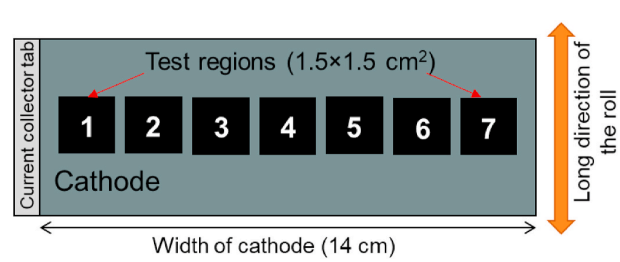

Fig. 7. Schematic of the tested regions in the cathode.

Ningde Amperex Tech. Exhibit No. 2030
Zhuhai CosMX Battery Co. Ltd. v. Ningde Amperex Tech.
IPR2025-00405, U.S. Patent No. 11,769,910
Page 7 of 9

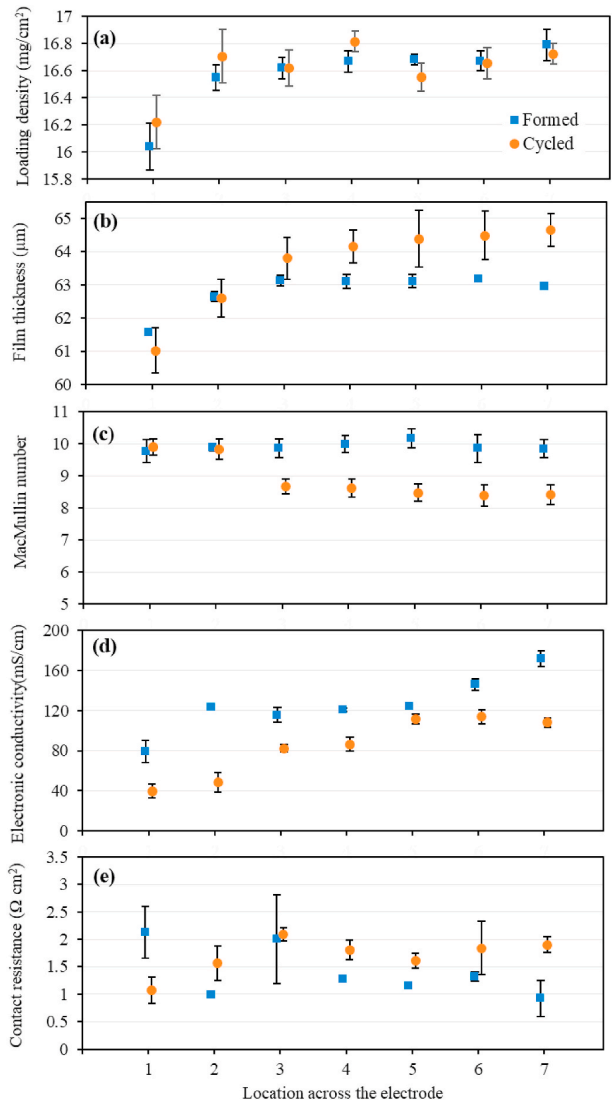

Fig. 8. TMO cathode formed and cycled results as a function of position for (a) loading density, (b) film thickness, (c) MacMullin number, (d) electronic conductivity, and (e) contact resistance.

harvested from different cell formats to investigate cycling effects on the ionic and electronic transport of the electrode. An increase in the thickness was observed for the formed and cycled electrodes. This observation can be related to general mechanical degradation and loss of adhesion among particles and between particles and the current collector.

The apparent capacity decreased during cell cycling, which can be partially ascribed to an internal impedance growth, one of the common signs of battery aging. We observed a significant degradation of electronic pathways as cycling proceeded. Surprisingly, our results show relatively stable values in MacMullin Number for all electrodes and even a modest improvement in ionic pathways for some electrodes during aging. One possible mechanism for the observed changes in electronic and ionic properties is that as cycling proceeds, the electrode structure undergoes mechanical stress due to changes in volume as ions are inserted and removed. This can cause particle cracking and binder degradation and detachment leading to electrode swelling and motion of active particles as well as carbon additive. During this process, the solvent can get in between particles and cracks and form additional SEI. Another possible mechanism hypothesized by Steingart and coworkers is gas evolution during cycling, leading to displacement of solvent and possible wetting of previously unwetted regions in the electrodes [53]. While such processes have a detrimental effect on the electronic conductivity due to loss of contact between particles and formation of additional SEI, they can make electrodes less tortuous by opening pores and creating new pathways for ions to travel. Therefore, it appears that the cell resistance growth, which can manifest as a capacity loss at finite charge and discharge rates, is not generally due to an increase in tortuosity. Instead, the degradation of electronic pathways may have a larger adverse effect than do the improvements in ionic pathways, leading to an increase in the overall impedance. This could explain why, as a general principle, the electronic conductivity at cell beginning of life is designed to be much greater than corresponding ionic conductivity, as electronic pathways are subject to greater losses over time. While having higher electrode conductivities (electronic or ionic) could be considered beneficial in terms of cell power density, they each come at a cost in terms of reallocated electrode volume toward inactive components (e.g. carbon additive or pores) leading to loss of energy density.

An inverse relationship or tradeoff between ionic and electronic conductivities might be expected but is not always observed. Under accelerated cycling at high temperature and high voltage, the LCO cathode showed deterioration in both ionic and electronic pathways. Aggressive cycling conditions can promote side reactions and surface film formation; it is not clear however what paricular phenomenon might explain the ionic pathway deterioration.

The NCM cathode showed a different ionic conductivity trend under cycling at a higher temperature compared to room temperature. These observations confirm that high-temperature cycling promotes other mechanisms that can deteriorate ionic pathways. Therefore, cycling at higher temperatures may not be an accurate extrapolation of a cell cycled at room temperature.

Cycling of the graphite anode based on water-soluble binder showed a decrease in electronic conductivity and an increase in ionic conductivity. The contact resistance also increased. Although an SEI layer may grow and deteriorate ionic pathways and reduce the corresponding conductivity, it does not seem to be a significant factor here. Instead, mechanical degradation continues to improve ionic conductivity during cycling. Anode cycling at elevated temperature followed the trend at room temperature; hence there was no indication of a different mechanism involved at higher temperature.

The LFP cathodes appear to maintain good stability of ionic and electronic conductivities after long-term cycling at least at room temperature. This result suggests that the proper choice of material and good cell design can help to mitigate many of the above-discussed structural changes.

This work shows that changes in ionic and electronic conductivities are strongly dependent on cell chemistry and cycling conditions. Although the choices of cell chemistry and cycling conditions depend on the application of the battery, alleviating degradation by revising cell design is being pursued by many researchers. For example, using a proper electrolyte package could help with surface film formation, or a proper binder system can help to provide a good electronic connection between particles during repetitive cycling.

CRediT authorship contribution statement

Fezzeh Pouraghajan: Investigation, writing. **Andrea I. Thompson:** Investigation. **Emilee E. Hunter:** Investigation. **Brian Mazzeo:** Supervision, editing. **Jake Christensen:** Investigation, editing. **Ram Subbaraman:** Investigation. **Michael Wray:** Investigation. **Dean Wheeler:** Supervision, writing.

Ningde Amperex Tech. Exhibit No. 2030
Zhuhai CosMX Battery Co. Ltd. v. Ningde Amperex Tech.
IPR2025-00405, U.S. Patent No. 11,769,910
Page 8 of 9

Declaration of competing interest

The authors declare that they have no known competing financial interests or personal relationships that could have appeared to influence the work reported in this paper.

Acknowledgements

Funding for this research was partially provided through the BMR project of the US Department of Energy. We would also like to acknowledge Chisu Kim of Hydro- Québec for providing electrodes for testing.

Appendix A. Supplementary data

Supplementary data to this article can be found online at https://doi.org/10.1016/j.jpowsour.2021.229636.

References

[1] A. Barré, et al., A review on lithium-ion battery ageing mechanisms and estimations for automotive applications, J. Power Sources 241 (2013) 680–689.
[2] M. Dubarry, N. Qin, P. Brooker, Calendar aging of commercial Li-ion cells of different chemistries–A review, Current Opinion in Electrochemistry 9 (2018) 106–113.
[3] M. Broussely, et al., Aging mechanism in Li ion cells and calendar life predictions, J. Power Sources 97 (2001) 13–21.
[4] M. Broussely, et al., Main aging mechanisms in Li ion batteries, J. Power Sources 146 (1–2) (2005) 90–96.
[5] D. Zhang, et al., Studies on capacity fade of lithium-ion batteries, J. Power Sources 91 (2) (2000) 122–129.
[6] G. Ning, B. Haran, B.N. Popov, Capacity fade study of lithium-ion batteries cycled at high discharge rates, J. Power Sources 117 (1–2) (2003) 160–169.
[7] X. Zhou, et al., Impedance characterization of lithium-ion batteries aging under high-temperature cycling: importance of electrolyte-phase diffusion, J. Power Sources 426 (2019) 216–222.
[8] B. Stiaszny, et al., Electrochemical characterization and post-mortem analysis of aged LiMn2O4–Li (Ni0. 5Mn0. 3Co0. 2) O2/graphite lithium ion batteries. Part I: cycle aging, J. Power Sources 251 (2014) 439–450.
[9] W. Waag, S. Käbitz, D.U. Sauer, Experimental investigation of the lithium-ion battery impedance characteristic at various conditions and aging states and its influence on the application, Appl. Energy 102 (2013) 885–897.
[10] M. Kabir, D.E. Demirocak, Degradation mechanisms in Li-ion batteries: a state-of-the-art review, Int. J. Energy Res. 41 (14) (2017) 1963–1986.
[11] P. Arora, R.E. White, M. Doyle, Capacity fade mechanisms and side reactions in lithium-ion batteries, J. Electrochem. Soc. 145 (10) (1998) 3647–3667.
[12] G. Sarre, P. Blanchard, M. Broussely, Aging of lithium-ion batteries, J. Power Sources 127 (1–2) (2004) 65–71.
[13] M. Wohlfahrt-Mehrens, C. Vogler, J. Garche, Aging mechanisms of lithium cathode materials, J. Power Sources 127 (1–2) (2004) 58–64.
[14] J. Vetter, et al., Ageing mechanisms in lithium-ion batteries, J. Power Sources 147 (1–2) (2005) 269–281.
[15] V. Agubra, J. Fergus, Lithium ion battery anode aging mechanisms, Materials 6 (4) (2013) 1310–1325.
[16] J. Christensen, J. Newman, Stress generation and fracture in lithium insertion materials, J. Solid State Electrochem. 10 (5) (2006) 293–319.
[17] D. Liu, et al., On the stress characteristics of graphite anode in commercial pouch lithium-ion battery, J. Power Sources 232 (2013) 29–33.
[18] D. Kong, et al., Study on degradation behavior of commercial 18650 LiAlNiCoO2 cells in over-charge conditions, Int. J. Energy Res. 43 (1) (2019) 552–567.
[19] Y. Itou, Y. Ukyo, Performance of LiNiCoO2 materials for advanced lithium-ion batteries, J. Power Sources 146 (1–2) (2005) 39–44.
[20] Y. Hu, X. Zhao, Z. Suo, Averting cracks caused by insertion reaction in lithium–ion batteries, J. Mater. Res. 25 (6) (2010) 1007–1010.
[21] J. Christensen, J. Newman, A mathematical model of stress generation and fracture in lithium manganese oxide, J. Electrochem. Soc. 153 (6) (2006) A1019–A1030.
[22] K. Zhao, et al., Fracture of electrodes in lithium-ion batteries caused by fast charging, J. Appl. Phys. 108 (7) (2010), 073517.
[23] X. Wang, et al., Understanding volume change in lithium-ion cells during charging and discharging using in situ measurements, J. Electrochem. Soc. 154 (1) (2007) A14–A21.
[24] L. Yang, B. Ravdel, B.L. Lucht, Electrolyte reactions with the surface of high voltage LiNi0. 5Mn1. 5O4 cathodes for lithium-ion batteries, Electrochem. Solid State Lett. 13 (8) (2010) A95–A97.
[25] C. Zhan, et al., Dissolution, migration, and deposition of transition metal ions in Li-ion batteries exemplified by Mn-based cathodes–a critical review, Energy Environ. Sci. 11 (2) (2018) 243–257.
[26] C. Delacourt, et al., Effect of manganese contamination on the solid-electrolyte-interphase properties in Li-ion batteries, J. Electrochem. Soc. 160 (8) (2013) A1099–A1107.
[27] J.A. Gilbert, I.A. Shkrob, D.P. Abraham, Transition metal dissolution, ion migration, electrocatalytic reduction and capacity loss in lithium-ion full cells, J. Electrochem. Soc. 164 (2) (2017) A389–A399.
[28] L. Bodenes, et al., Lithium secondary batteries working at very high temperature: capacity fade and understanding of aging mechanisms, J. Power Sources 236 (2013) 265–275.
[29] K. Striebel, et al., The development of low cost LiFePO4-based high power lithium-ion batteries, J. Power Sources 146 (1–2) (2005) 33–38.
[30] F. Pouraghajan, et al., Quantifying tortuosity of porous Li-ion battery electrodes: comparing polarization-interrupt and blocking-electrolyte methods, J. Electrochem. Soc. 165 (11) (2018) A2644–A2653.
[31] J. Landesfeind, et al., Tortuosity determination of battery electrodes and separators by impedance spectroscopy, J. Electrochem. Soc. 163 (7) (2016) A1373–A1387.
[32] B.J. Lanterman, et al., Micro-four-line probe to measure electronic conductivity and contact resistance of thin-film battery electrodes, J. Electrochem. Soc. 162 (10) (2015) A2145–A2151.
[33] E. Hardy, The Impact of Calendering on the Electronic Heterogeneity of Lithium-Ion Electrode Films, M.S. Thesis, Brigham Young University, Provo, Utah, USA, 2020.
[34] J.D. Flygare, et al., Mathematical model of four-line probe to determine conductive properties of thin-film battery electrodes, J. Electrochem. Soc. 162 (10) (2015) A2136–A2144.
[35] D.E. Stephenson, et al., Modeling 3D microstructure and ion transport in porous Li-ion battery electrodes, J. Electrochem. Soc. 158 (7) (2011) A781–A789.
[36] N.A. Zacharias, et al., Direct measurements of effective ionic transport in porous Li-ion electrodes, J. Electrochem. Soc. 160 (2) (2013) A306–A311.
[37] S.W. Peterson, D.R. Wheeler, Direct measurements of effective electronic transport in porous Li-ion electrodes, J. Electrochem. Soc. 161 (14) (2014) A2175–A2181.
[38] J.E. Vogel, et al., Electrode microstructure controls localized electronic impedance in li-ion batteries, Electrochim. Acta 297 (2019) 820–825.
[39] K. Jalkanen, et al., Cycle aging of commercial NMC/graphite pouch cells at different temperatures, Appl. Energy 154 (2015) 160–172.
[40] J. Shim, et al., Electrochemical analysis for cycle performance and capacity fading of a lithium-ion battery cycled at elevated temperature, J. Power Sources 112 (1) (2002) 222–230.
[41] J.-N. Zhang, et al., Dynamic evolution of cathode electrolyte interphase (CEI) on high voltage LiCoO2 cathode and its interaction with Li anode, Energy Storage Materials 14 (2018) 1–7.
[42] A. Guerfi, et al., LiFePO4 water-soluble binder electrode for Li-ion batteries, J. Power Sources 163 (2) (2007) 1047–1052.
[43] J. Choi, et al., Improved high-temperature performance of lithium-ion batteries through use of a thermally stable co-polyimide-based cathode binder, J. Power Sources 252 (2014) 138–143.
[44] T. Yoon, et al., Failure mechanisms of LiNi0. 5Mn1. 5O4 electrode at elevated temperature, J. Power Sources 215 (2012) 312–316.
[45] S. Jaiser, et al., Investigation of film solidification and binder migration during drying of Li-Ion battery anodes, J. Power Sources 318 (2016) 210–219.
[46] F. Font, et al., Binder migration during drying of lithium-ion battery electrodes: modelling and comparison to experiment, J. Power Sources 393 (2018) 177–185.
[47] F.L. Usseglio-Viretta, et al., Resolving the discrepancy in tortuosity factor estimation for li-ion battery electrodes through micro-macro modeling and experiment, J. Electrochem. Soc. 165 (14) (2018) A3403–A3426.
[48] Y.S. Hu, et al., Synthesis of hierarchically porous carbon monoliths with highly ordered microstructure and their application in rechargeable lithium batteries with high-rate capability, Adv. Funct. Mater. 17 (12) (2007) 1873–1878.
[49] I.V. Thorat, et al., Quantifying tortuosity in porous Li-ion battery materials, J. Power Sources 188 (2) (2009) 592–600.
[50] J.H. Lee, H.M. Lee, S. Ahn, Battery dimensional changes occurring during charge/discharge cycles—thin rectangular lithium ion and polymer cells, J. Power Sources 119 (2003) 833–837.
[51] R. Kostecki, F. McLarnon, Microprobe study of the effect of Li intercalation on the structure of graphite, J. Power Sources 119–121 (2003) 550–554.
[52] V.A. Sethuraman, et al., Surface structural disordering in graphite upon lithium intercalation/deintercalation, J. Power Sources 195 (11) (2010) 3655–3660.
[53] Kevin Knehr, et al., Understanding full-cell evolution and non-chemical electrode crosstalk of Li-ion batteries, Joule 2 (6) (2018) 1146–1159.

Ningde Amperex Tech. Exhibit No. 2030
Zhuhai CosMX Battery Co. Ltd. v. Ningde Amperex Tech.
IPR2025-00405, U.S. Patent No. 11,769,910
Page 9 of 9